Published in final edited form as:
Bioconjug Chem. 2013 February 20; 24(2): 196–204. doi:10.1021/bc300473x.

Nanoparticle PET/CT Imaging of Natriuretic Peptide Clearance Receptor in Prostate Cancer

Eric D. Pressly[†], **Richard A. Pierce**[‡], **Luke A. Connal**[†], **Craig J. Hawker**[†,#], and **Yongjian Liu**[§,*]

[†]Materials Research Laboratory, University of California, Santa Barbara, California 93106, United States

[#]Materials Department and Department of Chemistry, and Biochemistry, University of California, Santa Barbara, California 93106, United States

[‡]Department of Medicine, Washington University, St. Louis, Missouri 63110, United States

[§]Department of Radiology, Washington University, St. Louis, Missouri 63110, United States

Abstract

Atrial natriuretic peptide has been recently discovered to have anticancer effects *via* interaction with cell surface natriuretic peptide receptor A (NPRA) and natriuretic peptide clearance receptor (NPRC). In a preclinical model, NPRA expression has been identified during the tumor angiogenesis and may serve as a potential prognostic marker and target for prostate cancer (PCa) therapy. However, the presence of NPRC receptor in PCa model has not yet been assessed. Furthermore, there is still no report using nanoparticle for PCa positron emission tomography (PET) imaging. Herein, an amphiphilic comb-like nanoparticle was synthesized with controlled properties through modular construction containing C-atrial natriuretic factor (CANF) for NPRC receptor targeting and 1,4,7,10-tetraazacyclododecane-1,4,7,10-tetraacetic acid (DOTA) chelator for high specific activity Cu-64 radiolabeling. The pharmacokinetics of ^{64}Cu-CANF-Comb exhibited tuned biodistribution and optimized *in vivo* profile in contrast to the non-targeted ^{64}Cu-Comb nanoparticle. PET imaging with ^{64}Cu-CANF-Comb in CWR22 PCa tumor model showed high blood pool retention, low renal clearance, enhanced tumor uptake, and decreased hepatic burden relative to the non-targeted ^{64}Cu-Comb. Immunohistochemistry staining confirmed the presence of NPRC receptor in tumor tissue. Competitive PET receptor blocking study demonstrated the targeting specificity of ^{64}Cu-CANF-Comb to NPRC receptor *in vivo*. These results establish a new nanoagent for prostate cancer PET imaging.

Keywords

Prostate cancer; natriuretic peptide clearance receptor; nanoparticle; positron emission tomography; imaging

Corresponding author: Yongjian Liu, Ph.D., Department of Radiology, Washington University, Campus Box 8225, 510 S. Kingshighway Blvd., St. Louis, MO 63110, liuyo@mir.wustl.edu, Phone: 314-362-8431, Fax: 314-362-9940.

In memory of Professor Michael J. Welch, a leading PET imaging scientist and strong supporter of this research who passed away on May 6th, 2012.

No other potential conflict of interest relevant to this article was reported.

INTRODUCTION

Prostate cancer (PCa) is the most common noncutaneous malignancy affecting men in the US, with 241,740 estimated new cases resulting in approximately 28,170 deaths in 2012.[1] With the widespread use of screening tests (for example, prostate-specific-antigen testing), patients are diagnosed with less-advanced disease and the prostate-cancer-specific mortality has declined over the past few years. This has shifted the focus of treatment from whole-gland to focal therapy owing to the multifocal nature of prostate cancer.[2] Thus, specific and sensitive imaging becomes the key for early diagnosis, staging, and monitoring of treatment response.

Clinically, many imaging modalities have been used for PCa detection and staging including transrectal ultrasound, magnetic resonance imaging (MRI), computed tomography (CT), single photon emission computed tomography (SPECT), and positron emission tomography (PET).[3] Among them, MRI provides the highest spatial resolution and allows the best depiction of the internal zone anatomy of the prostate as well as its contours. Lately, with the advance of functional MRI such as dynamic contrast-enhanced MRI, MRI can also be used for PCa detection and staging.[4] However, radiotracer based imaging modalities, especially PET and PET/CT are still favored owing to the high sensitivity and functional imaging which enables the early detection and monitoring the physiological process during PCa development.[5] Currently, the most common radiotracer for clinical PET imaging, [^{18}F]-fluoro-2-deoxy-2-D-glucose ([^{18}F]-FDG), is not effective in the diagnosis of localized prostate cancer because of PCa's glucose independent metabolism.[6] Other tracers used for clinical research such as ^{18}F/^{11}C-choline or ^{11}C-acetate have shown promise in early studies, but the results need to be evaluated further in larger prospective clinical trials. Still, none of these tracers is PCa specific.

In the development of PET imaging probes for PCa, the majority of studies have focused on the use of small molecule based tracers such as prostate-specific membrane antigen targeting molecules or gastrin-releasing peptide receptor targeted probes.[7–13] However, most of these had fast renal clearance and therefore low tumor uptakes, which may limit the potential for translational research. Nanoparticles, thanks to the unique physicochemical properties such as multivalency and multifunctionality, have been widely used for various cancer diagnosis and therapy [14–17] including PCa.[18–20] Currently, there are few studies of nanoagents for PCa PET imaging.

Natriuretic peptide is a group of cardiac hormones that play an important role in vasodilation, cardiovascular homeostasis, sodium excretion and inhibition of aldosterone secretion by interacting with their receptors.[21] Additionally, they have been reported to have other physiologic effects such as involvement in immunity and inflammation. [22] Lately, atrial natriuretic peptide (ANP) has been reported imparting an anticancer effect *via* interaction with cell surface natriuretic peptide receptor A (NPRA) and natriuretic peptide clearance receptor (NPRC).[22–25] NPRA expression has been well characterized during the tumor angiogenesis process and might serve as a potential prognostic marker and target for PCa imaging and therapy. [22,25] Interestingly, NPRC receptor was also identified in human prostate carcinoma cells and its gene expression was confirmed in mouse xenograft model. [26,27] Since the NPRC receptor population accounts for approximately 95% of all natriuretic peptide receptors, hence imaging the up-regulation of NPRC receptor in PCa model could identify a powerful target for early detection of PCa.

In the current study, a nanoparticle was designed and synthesized with a controlled loading of NPRC targeting peptide C-type atrial natriuretic factor (CANF) and 1,4,7,10-tetraazacyclododecane-1,4,7,10-tetraacetic acid (DOTA) chelator for ^{64}Cu radiolabeling.

We have investigated the use of this well-defined polymeric nanoparticle for *in vivo* pharmacokinetic evaluation and PET imaging in a mouse CWR22 prostate tumor model. The targeting specificity and imaging efficiency were compared with the control nanoparticles and confirmed with the use of small-animal PET/CT. This work identifies the up-regulation of NPRC receptor in PCa model which may serve as a new biomarker for future targeted cancer therapy.

EXPERIMENTAL SECTION

Materials

Chemicals were purchased from Sigma-Aldrich (St. Louis, MO, USA) and used without further purification unless otherwise stated, functionalized poly(ethylene glycol) (PEG) derivatives were obtained from Intezyne Technologies, (Tampa, FL, USA). ^{64}Cu was prepared on the Washington University Medical School CS-15 Cyclotron by the ^{64}Ni(p,n)^{64}Cu nuclear reaction at a specific activity of 50 – 200 mCi/μg (end of bombardment), as previously described.[35] The buffers used for ^{64}Cu-labeling were treated with Chelex-100 resin (Bio-Rad Laboratories, Hercules, CA, USA) before use. Tris-*t*-butylester-DOTA and 1,4,7,10-tetraazacyclododecane were purchased from Macrocyclics (Dallas, TX, USA). Centricon tubes (YM-30: MWCO 30 kDa; YM-50: MWCO 50 kDa; YM-100: MWCO 100 kDa) were purchased from Millipore. HiTrap Desalting columns (5 mL) were purchased from GE Healthcare Biosciences (Piscataway, NJ, USA). 2-(2-Bromoacetoxy)ethyl methacrylate,[36] dithiolester Radical Addition Fragmentation Transfer (RAFT) agent,[37] 1,4,7,10-Tetraazacyclododecane-1,4,7-tris(*t*-butyl acetate) (DO3A)[38] and 4-pentynoic anhydride[39] were prepared as previously reported. Vitronectin, fibronectin, $\alpha_v\beta_3$ and $\alpha_v\beta_5$ were purchased from Chemicon. Integrin $\alpha_{IIb}\beta_3$ was purchased from EMD Chemicals, Inc. (Gibbstown, NJ).

Polymeric materials were characterized by ^{1}H and ^{13}C nuclear magnetic resonance (NMR) spectroscopy using either a Bruker 200, 300 or 500 MHz spectrometer with the residual solvent signal as an internal reference. Gel permeation chromatography (GPC) was performed in DMF on a Waters system (Millford, MA, USA) equipped with four 5-mm Waters columns (300 × 7.7 mm) connected in series with increasing pore size (10^2, 10^3, 10^4, and 10^6 Å). Waters 410 differential refractometer index and 996 photodiode array detectors were employed. The molecular weights of the polymers were calculated relative to linear poly(ethylene oxide) standards. Fourier transformed infrared spectroscopy was performed using a Nicolet Magna 850 IR-Raman instrument on a CaF_2 salt plate. The spectra were acquired at a 4 cm^{-1} resolution and 128 scans. A Bioscan 200 imaging scanner (Bioscan, Washington, DC, USA) was used to read the instant thin layer chromatography (ITLC) plates (Pall ITLC-SG plates, VWR International, Batavia, IL, USA). Fast protein liquid chromatography (FPLC) and radio-FPLC were performed using an AKTA FPLC system (GE Healthcare Biosciences) equipped with a Beckman 170 Radioisotope Detector (Beckman Instruments, Fullerton, CA, USA).

Synthesis of DOTA methacrylate (DOTA-MA)

DO3A (1.92 g, 3.74 mmol) and 2-(2-bromoacetoxy)ethyl methacrylate (1.02 g, 4.06 mmol) were dissolved in acetonitrile (50 mL) followed by the addition of K_2CO_3 (0.62 g, 4.48 mmol) and the reaction mixture was then stirred overnight at RT. Dichloromethane (50 mL) was added to the reaction which was extracted with water (25 mL), concentrated by rotary evaporation and purified by flash chromatography (DCM:MeOH, 95:5) to obtain a viscous clear oil (yield 1.81 g, 71%); ^{1}H NMR (500 MHz, $CDCl_3$) δ 6.14 (s, 1H), 5.63 (s, 1H), 4.39 (d, J = 19.1 Hz, 4H), 3.98 – 2.05 (m, 22H), 1.96 (s, 3H), 1.47 (t, J = 6.7 Hz, 27H). The

product was anayzed with ESI-TOF mass spectrometry. (m/z): [M]+ calcd. 684.43, $C_{34}H_{60}N_4O_{10}$; found 684.53.

Synthesis of poly(ethylene glycol) methyl ether methacrylate (PEGMA)

5.0 kDa poly(ethylene glycol) monomethyl ether (mPEG, 5.00 g, 1.00 mmol) was dissolved in dichloromethane (25 mL) and triethylamine (5 mL). Freshly distilled methacryloyl chloride (5.00 ml, 5.35 g, 5.12 mmol) was added dropwise at 0°C and the reaction mixture was allowed to stir overnight under argon. The reaction was quenched with water, filtered and the organic phase washed with 10% $NaHSO_4$ (w/v), dried over anhydrous $MgSO_4$, and concentrated in vacuum to *ca*. 10 mL. The product was precipitated by adding cold diethyl ether (200 mL) and dried in vacuum (4.65 g, 92%); ^{1}H NMR ($CDCl_3$, 200 MHz), δ (ppm): 6.15 (1H), 5.58 (1H), 4.32 (2H), 3.6 (450H), 1.95 (2H); M_n= 5.1 kDa. PDI: 1.03.

Synthesis of azido poly(ethylene glycol) methacrylate (N_3-PEGMA)

5.0 kDa poly(ethylene glycol) mono-azide (1.50 g, 0.30 mmol) was dissolved in dichloromethane (15 mL) and triethylamine (3 mL). Freshly distilled methacryloyl chloride (0.70 mL, 0.75 g, 7.1 mmol) was added dropwise at 0°C and the reaction mixture was allowed to stir overnight under argon. The reaction was quenched with water, filtered and the organic phase washed with 10% $NaHSO_4$ (w/v), dried over anhydrous $MgSO_4$, and concentrated in vacuum to ca. 3 mL. The product was precipitated by adding cold diethyl ether (100 mL) and dried in vacuum (yield 1.11 g, 74%); ^{1}H NMR (500 MHz, CD_2Cl_2) δ 6.13 (s, 1H), 5.61 (s, 1H), 4.35 – 4.26 (m, 2H), 3.78 – 3.57 (m, 464H), 3.53 – 3.45 (m, 3H), 3.42 (t, J = 5.0 Hz, 2H), 1.97 (s, 3H); M_n= 5.1 kDa. PDI: 1.03.

Synthesis of Acteylene-CANF—CANF (59.3 mg, 0.037 mmol) was dissolved in 2mL anhydrous DMF and 4-pentynoic anhydride (19.2 mg, 0.098 mmol) dissolved in 1.5 mL anhydrous DMF was added dropwise to the solution and allowed to stir 2 days. Cold diethyl ether (15 mL) was added to the solution to triturate the product, which was subsequently dissolved in 2 mL of MilliQ water and freeze dried (yield 47.0 mg, 75%); M_w(ESI) 1674.73 {M+H$^+$] (calc. 1674.80).

Synthesis of poly(ethylene glycol) CANF methacrylate (CANF-PEGMA)—N_3-PEGMA (75.4 mg, 0.015 mmol) and Acetylene-CANF (42.8 mg, 0.025 mmol) were dissolved in a solution of 1.0 g DMSO and 0.65 g MilliQ water followed by the additions of 50 μL 5wt% aqueous CuSulfate (0.018 mmol) and 75 μL 5wt% aqueous NaAscorbate (0.016 mmol), respectively. The reaction was allowed to stir for two days with repeat additions of $CuSO_4$ (50 μL) and NaAscorbate (75 μL) solutions after one day. The product was purified by washing (10×) with MilliQ water in 15 mL centricon tubes (YM-5) and freeze-dried (yield 48 mg, 41%) (see Figure S1 for NMR (DMSO-d_6), FT-IR, ν (cm^{-1}): 3315, 2881, 1655, 1466, 1342, 1099, 962, 841. GPC M_n 6500, PDI 1.1 (PMMA standards, DMF).

Synthesis of comb copolymers

The synthesis of comb polymers was adapted from a previous report[29] with the exception of DOTA methacrylate and poly(ethylene glycol) CANF methacrylate being incorporated into the polymerization mixture. To illustrate: PEGMA 5.0 kDa (205 mg, 0.041 mmol), CANF-PEGMA (100 mg, 0.015 mmol), methyl methacrylate (MMA) (43.6 mg, 0.51 mmol), azobisisobutyronitrile (AIBN) (0.069 mg, 0.00042 mmol), DOTA-MA (22.2 mg, 0.032 mmol), and RAFT agent (0.33 mg, 0.0011 mmol) were dissolved in DMF (1.99 g). AIBN, DOTA-MA and RAFT agent were added as DMF stock solutions. The solution was transferred to a 5 mL Schlenk flask and three freeze-pump-thaw cycles performed before being heated at 70 °C for 120 h. Following the polymerization, the solution was diluted with

DMF, transferred to four 15 mL centricon tubes (YM-50) and extensively washed with DMF, removal of monomers monitored by GPC. The copolymer was then washed with MilliQ water (5×) and freeze-dried to give the desired graft copolymer as a white powder (Yield 68 mg); M_n 205 kDa, PDI 1.20 and M_n 220 kDa, PDI 1.25 for CANF-Comb and control Comb respectively, (GPC-DMF, PMMA standards)[28]

DOTA deprotection and formation of nanoparticles

After removal of t-butyl protecting groups,[29] the polymers were dissolved in DMSO (1 wt %), a rapid addition of an equal aliquot achieved assembly, and DMSO was removed by centrifugal filtration, resulting in particles of 16 nm and 22 nm (dynamic light scattering) for the targeting CANF-Comb (zeta potential: −1.1 ± 1 mV) and non-targeting Comb (zeta potential: −35 ± 4 mV) particles, respectively (Scheme 1). After centrifugal filtration cycles with MilliQ water (3 ×), the nanoparticle were reconstituted in water (ca. 3 mg/mL) and stored at 4 °C for further use.

CWR22 Mouse Prostate Cancer Model—All animal studies were performed in compliance with guidelines set forth by the NIH Office of Laboratory Animal Welfare and were approved by the Washington University Animal Studies Committee. CWR22 model, an androgen dependent xenograft model derived from a primary human prostatic carcinoma,[30] has been widely used for various PCa treatment studies. [31,32] Since the purpose of this study was to identify NPRC as a new PCa biomarker for PET imaging and serve as a foundation for future targeted therapy study, CWR22 model was selected. Briefly, four- to 6-wk-old athymic nu/nu male mice were obtained from Charles River Laboratories. The CWR22 tumor line was a gift from Dr.Thomas G. Pretlow (Case Western Reserve University, Cleveland, OH). The CWR22 tumor was propagated in the animals by the implantation of minced tumor tissue, from a previously established tumor, into the subcutaneous tissue of the right flank of the mice.[33] Six to eight weeks after implantation, the tumor grew to about 700 –1000 mm^3 and then the mice were injected intravenously with the developed nanoparticles. The growth curve of the CWR22 tumor bearing mice was illustrated in figure S2.

Copper-64 radiolabeling of CANF-Comb and Comb—The ^{64}Cu (half-life = 12.7 h, β^+ = 17%, β^- = 40%) was produced at the Washington University cyclotron facility by the ^{64}Ni (p,n) ^{64}Cu nuclear reaction at a specific activity of 1.85–7.40 GBq/μg at the end of bombardment. [34,35] The Cu-64 radiolabeling procedure for the two nanoparticles followed the reported procedure. Briefly, the targeted CANF-Comb and non-targeted Comb (5 μg, about 5 pmol) were incubated with 185 MBq ^{64}Cu in 200 μL 0.1 M pH 5.5 ammonium acetate buffer at 80 °C for 1 h, respectively. After ethylene diamine tetraacetic acid (EDTA, 10 mM in 50 mM pH 7.4 phosphate buffer) challenge, the ^{64}Cu-CANF-Comb and ^{64}Cu-Comb were separated from ^{64}Cu-EDTA with 2 mL zeba spin desalting column. The radiochemical purity of the labeled nanoprobe was measured by radioactive thin layer chromatography (Radio-TLC) (Washington DC).

Bio-Distribution Studies—^{64}Cu-CANF-Comb and ^{64}Cu-Comb were reconstituted in 0.9% sodium chloride (APP pharmaceuticals) for intravenous (i.v.) injection. Male CWR22 mice weighing 25–32 g (n=24) were anesthetized with inhaled isoflurane and about 370 kBq of labeled nanoparticles (~ 4.0 μg/kg body weight) in 100 μL saline were injected *via* the tail vein. The mice were re-anesthetized before euthanizing them by cervical dislocation at each time point (1 h, 4 h, and 24 h) post injection (p.i.). Organs of interest were collected, weighed, and counted in a well gamma counter (Beckman 8000, San Diego, CA). Standards were prepared and measured along with the samples to calculate the percentage of the

injected dose per gram of tissue (%ID/gram) or percentage of the injected dose per organ of tissue (%ID/organ).[36]

PET/CT Imaging—About 6 weeks after the tumor implantation, CWR22 tumor-bearing mice were anesthetized with isoflurane and injected i.v. with 3.7 MBq/100 μL of ^{64}Cu labeled nanoparticles *via* the tail vein. The microPET images (corrected for attenuation, scatter, normalization and camera dead time) sessions were carried out on an Inveon PET/CT system (Siemens Medical Solutions, Knoxville, TN) and microPET Focus 220 at 1 h (one 15-min frame), 4 h (one 30-min frame) and 24 h p.i. (one 60-min frame). All the PET scanners were cross-calibrated periodically. The microPET images were analyzed with ASIPro.[37] The tumor uptake of ^{64}Cu-CANF-Comb was calculated in terms of the mean standardized uptake value (SUV) in three-dimensional (3D) regions of interest (ROIs). In general, SUV is defined as the tissue concentration of radiotracer divided by the activity injected per body weight and is calculated according to the following equation. The SUV data was not corrected for partial volume effects.[38]

$$\mathrm{SUV}=\frac{\text{radioactivity concentrat ion in ROI[Bq/mL]}}{\text{injected}\,\frac{\text{dose[Bq]}}{\text{animal weight[g]}}}$$

After the PET imaging, the animals were euthanized by cervical dislocation and the tumors were fixed *in situ* with freshly prepared 4% paraformaldehyde (Electron Microscopy Science Inc, Hatfield, PA.) for histopathology and immunohistochemistry.

Competitive Receptor Blocking Studies—Competitive PET receptor blocking studies were performed in CWR22 tumor-bearing mice (27.9 ± 2.9 g) with co-injection of non-radiolabeled CANF-Comb and ^{64}Cu-CANF-Comb with 100:1 mole ratio for both bio-distribution and PET/CT imaging studies.

Immunohistochemistry—Tumor tissue specimens were fixed in the 4% paraformaldehyde right after the collection, stored overnight at 4 °C, and then embedded in paraffin and sectioned at 5 microns for immunohistochemistry. Following de-waxing and hydration, sections were heated in 10 mM sodium citrate pH 6.0 with 0.1% Tween for 15 minutes at boiling temperature for antigen retrieval. Following blocking with non-immune serum, sections were incubated with Genway (San Diego, CA) mouse monoclonal anti-NPRC antibody 4C3 overnight at 1:400 dilution using Vector Laboratories M.O.M. kit (Burlingame, CA). Color development employed Vector Laboratories Vectastain alkaline phosphatase ABC system (Burlingame, CA) and blue substrate, and sections were counterstained using nuclear fast red. Sections incubated with pre-immune serum and sections incubated with secondary antibody only gave no signal.

Statistical Analysis—Group variation is described as mean ± standard deviation. Group comparisons were made using student t-test. The significance level in all tests was $p \leq 0.05$. GraphPad Prism v. 5.02 (La Jolla, CA) was used for all statistical analyses.

RESULTS

Biodistribution in CWR22 tumor-bearing mice

Biodistribution results of the non-targeted nanoparticle ^{64}Cu-Comb in CWR22 tumor mice showed similar pharmacokinetics as were reported previously (Figure 1A in %ID/g, Figure S3A in %ID/organ).[39] The blood retention of ^{64}Cu-Comb showed a decreasing profile from 24.6 ± 1.41 %ID/g at 1 h p.i. to 8.28 ± 0.20 % ID/g at 24 h. The liver uptakes were dominant

during the whole study and increased over time from 25.8 ± 6.47% ID/g at 1 h to 37.1 ± 9.02%ID/g at 24 h. Interestingly, spleen accumulation dropped to about half of the initial uptake by 24 h. The other clearance of ^{64}Cu-Comb was through the kidney with ~ 10% ID/g across the study, relative to the low accumulation in gastrointestinal tract (stomach and intestines). Tumor uptake almost doubled during the 24 h study, which led to increased tumor-to-muscle (T/M) ratio and tumor-to-blood (T/B) ratio from 2.10 ± 0.72 and 0.06 ± 0.02 at 1 h to 7.50 ± 2.09 and 0.36 ±0.02 at 24 h, respectively.

The targeted ^{64}Cu-CANF-Comb showed a biodistribution profile superior to the non-targeted ^{64}Cu-Comb during the 24 h study (Figure 1B in %ID/g, Figure S3B in %ID/ogran). In contrast to the high and gradually increased reticuloendothelial system (RES) clearance of ^{64}Cu-Comb, the liver accumulation of ^{64}Cu-CANF-Comb progressively decreased during the study. At each time point, the liver accumulations of ^{64}Cu-CANF-Comb were all significantly ($p<0.05$, n=4) lower than those of non-targeted ^{64}Cu-Comb. Especially at 24 h, the liver uptake of ^{64}Cu-CANF-Comb was only 15% of that obtained with ^{64}Cu-Comb. Also, the blood retentions of ^{64}Cu-CANF-Comb were all higher ($p<0.0001$ at 1 h, n=4) than those of ^{64}Cu-Comb at each time point. More importantly, the tumor showed increasing localization of ^{64}Cu-CANF-Comb over time. The tracer uptake SUVs, T/M ratios and T/B ratios (0.12 ± 0.01, 0.36 ± 0.09, and 0.95 ± 0.13 at 1 h, 4 h and 24 h, respectively) at each time point were all significantly ($p<0.001$, n=4) higher than those obtained with the non-targeted ^{64}Cu-Comb.

PET/CT imaging

PET/CT images at 24 h clearly showed the tumor accumulation of ^{64}Cu-CANF-Comb in CWR22 tumor bearing mice, in contrast to the weak tumor accumulation observed with non-targeted ^{64}Cu-Comb (Figure 2). Interestingly, the bladder accumulation was very low for both ^{64}Cu-CANF-Comb and ^{64}Cu-Comb. Consistent with the bio-distribution results, ^{64}Cu-CANF-Comb showed higher heart accumulation and lower liver uptake than those obtained with ^{64}Cu-Comb. The quantitative analysis showed increased ^{64}Cu-CANF-Comb tumor localization over time (Figure 3A). At each time point, the tumor uptake and T/M ratio were all significantly ($p<0.05$, n=6–8) higher than corresponding data obtained with the non-targeted ^{64}Cu-Comb. Particularly at 24 h, ^{64}Cu-CANF-Comb had a three-fold more T/M ratio than the non-targeted ^{64}Cu-Comb (Figure 3 A, B).

Competitive receptor blocking

Competitive receptor blocking with co-injection of unlabeled CANF-Comb resulted in a substantial tumor uptake decrease while retaining similar *in vivo* pharmacokinetics profile. The organ uptakes (except for tumor) of the blocked group were all comparable to those obtained without blockade (Figure 4 in %ID/g, Figure S4 in %ID/organ). However, the tumor accumulation was significantly ($p<0.0001$, n=6) blocked from 9.19 ± 0.21%ID/g to 3.23 ± 1.15%ID/g. Consistent with bio-distribution blocking data, PET/CT image also clearly demonstrated the decreased tumor localization of ^{64}Cu-CANF-Comb (Figure 2). The quantitative analysis showed that the tumor uptake and T/M ratio were both significantly ($p<0.01$, n=6) reduced at each time point in the blocking group (Figure 3B).

Immunohistochemistry

Immunohistochemistry (IHC) showed the presence of cells positive for NPRC within and surrounding the tumor mass (Figure 5). The tumor cells were largely negative, but pools of NPRC positive inflammatory cells were found within the tumors (Figure 5 A, B) and lining blood vessels in stromal tissue surrounding the tumors (Figure 5 B, C). The control staining using a pre-immune serum instead of primary antibody confirmed the specificity of NPRC IHC (Figure 5D).

DISCUSSION

Herein, we have reported the synthesis, characterization and biological evaluation of ^{64}Cu-CANF-Comb, a nanoparticle for specific targeting of the NPRC receptor in human prostate cancer xenograft using *in vivo* biodistribution assay, small animal PET/CT imaging, as well as immunohistochemistry. This targeted nanoparticle exhibited improved pharmacokinetics with extended blood retention and low hepatic burden compared to the non-targeted ^{64}Cu-Comb nanoparticle. PET/CT imaging clearly showed the tumor uptake and confirmed the targeting specificity with blocking studies. The expression of NPRC receptor in tumor was also verified by IHC.

Radiolabeled peptides have been an effective way to target cellular receptors for *in vivo* diagnosis, characterization and targeted radiotherapy owing to the high sensitivity and specificity.[9] In PCa imaging, gastrin-releasing peptide receptor has been widely studied with bombesin analogs for PET. [7,8,10,13,40] However, most of these tracers have low tumor uptakes due to the fast renal clearance. Among them, ^{64}Cu-SarAr-SA-Aoc-bombesin (7–14) had the highest tumor uptake (~13%ID/g and ~7%ID/g at 1 h and 24 h, respectively) in all the ^{64}Cu labeled bombesin analogs.[7] Although the fast renal clearance lessened the concern of toxicity, it also led to low tumor/kidney (T/K) ratio (bladder was not collected), which might be an issue in further translational studies owing to possible interference on prostate tumor uptake quantification caused by high bladder accumulation of the radiotracer. Thus, an imaging probe with tuned *in vivo* pharmacokinetics and renal clearance, improved tumor uptake, and enhanced tumor-to-background ratio is necessary for clinical settings.

Nanoparticles, owing to the versatile physiochemical properties, can provide significant improvements in pharmacokinetics, targeting efficiency and specificity for oncological diagnosis, potentially leading to earlier detection and better treatment options for cancer.[41] In the design of nanoparticles for targeted cancer diagnosis, the controlled structure including size, surface properties, targeting group and radiolabeling site are important factors for *in vivo* imaging applications. In previous studies, the poly(methyl methacrylate)-core/PEG-shell amphophilic CANF-Comb nanoparticle has shown that its *in vivo* imaging capability could be accurately tailored by changing the molecular parameters of the starting functionalized copolymer.[39] Feed ratios were used to control the incorporation of various monomers as methacrylate have been shown to copolymerize randomly.[29] The DOTA chelator for ^{64}Cu and CANF targeting peptide could be precisely conjugated to the Comb nanoparticles (~ 105 DOTA/particle) to have controlled radiolabeling specific activity and targeting efficiency. In this study, CANF peptide end functionalized onto a PEG macromonomer was copolymerized with a non-functional PEG macromonomer to afford comb-like copolymers, these polymers were self-assembled in water to afford CANF-Comb nanopartilces with high CANF loading (~ 35 CANF/particle) for initial evaluation (Scheme 1). As previously reported, higher loading of targeting peptide would decrease the systemic circulation of nanoparticles. Although the 25% CANF-Comb nanoparticles used in this study had similar size and surface charge as those used in the previous study (10% CANF-Comb, 14 CANF/particle), its 1 h blood retention was about 60% of the 10% CANF-Comb nanoparticle despite animal species difference, reasonably owing to the conjugation of ~ 21 more CANF peptide (150% higher loading), which was also confirmed by the change of octanol-water distribution coefficient (log P) from −2.03 ± 0.02 (10% CANF-Comb, n=4) to less hydrophilic value of −1.47 ± 0.03 (25% CANF-Comb, n=4). This clearly showed the advantage of using this the poly(methyl methacrylate)-core/PEG-shell amphophilic nanoparticle to achieve tuned *in vivo* behavior through changing the molecular parameters of the starting functionalized copolymer.[39]

Previous studies had shown that neutral nanoparticles had extended *in vivo* blood retention and reduced hepatic and splenic accumulation compared to charged nanoparticles in similar size.[14] Herein, the surface charge effect was clearly illustrated. Compared to the neutral particle CANF-Comb (−1.1 ±1 mV), the negatively charged Comb nanoparticles (−35 ± 4 mV) showed less blood retention and gradually increased hepatic uptake during the 24 h study. For nanoparticle tumor targeting, one advantage is the well-known enhanced permeation and retention (EPR) effect due to the leaky vasculature of tumor and the size of nanoparticles, which was clearly observed for the non-targeted Comb nanoparticle with gradual increase over time (Figure 3). Although the elevated blood retention of CANF-Comb would cause more EPR effect in tumor uptake comparing to Comb nanoparticle, the accumulation of CANF-Comb in CWR22 tumor was largely due to the active targeting to the NPRC receptor, as confirmed by the higher CANF-Comb/Comb tumor uptake ratios (2.4–3.1) than those of blood retention ratios (1.2–1.3). Further, the biodistribution blocking studies also verified the NPRC receptor specific uptake, which showed similar ^{64}Cu-CANF-Comb uptakes in all the organs except for 2-fold decrease in tumor due to the nonradiolabeled CANF-Comb blockade. In the PET imaging study, the high specific activity (3.7 ± 1.1 GBq/nmol) of ^{64}Cu-CANF-Comb ensured only picomole level of radiotracer for *in vivo* application and minimal self-blocking effect, leading to high contrast and accurate quantification. The ^{64}Cu-CANF-Comb PET image clearly showed the high tumor localization and low liver accumulation (Figure 2). For the non-targeted ^{64}Cu-Comb nanoparticle, although tumor uptake was observed and increased along the study period (Figures 2, 3), it is still significantly lower than that of ^{64}Cu-CANF-Comb at each time point. Again, the PET blocking study of ^{64}Cu-CANF-Comb, consistent with the biodistribution study, clearly showed the substantial decrease in tumor accumulation to a level similar to the non-targeted ^{64}Cu-Comb, indicating the NPRC mediated tumor uptake (Figures 2, 3). Interestingly, the heart accumulation of ^{64}Cu-CANF-Comb did not change significantly with CANF-Comb blockade, indicating the uptake in heart was mainly owing to the blood pool retention. Compared to the other reported PCa PET tracer,[12] ^{64}Cu-CANF-Comb showed sufficient T/M ratio (21.0 ± 3.4, n=6–8) at 24 h and a higher T/K ratio (2.3 ± 0.2, n=6–8), indicating the advantage of nanoparticles for PCa imaging and the potential for translational research. Additionally, the higher T/M and T/B ratios of ^{64}Cu-CANF-Comb than those of ^{64}Cu-Comb and ^{64}Cu-CANF-Comb blocking at the three time points also confirmed the NPRC receptor specific tracer accumulation.

Since the recently discovered anticancer property of ANP,[23–25] NPRA has been demonstrated as a potential prognostic marker and a target for PCa therapy. NPRC receptor, though traditionally viewed as a clearance receptor of natriuretic peptide, occupies a large population (>95%) of the NPR family and has recently been implicated in more pathophysiological roles in human diseases.[42] Although the presence of NPRC receptor was identified in human PC-3 prostate carcinoma cells and mouse KUCaP-2 xenograft model, there was lack of information about its detailed characterization and localization in the tumor and potential for PCa diagnosis. In this study, IHC staining clearly showed the up-regulation of NPRC receptor in both tumor margin (possibly inflammatory cells and endothelial) and the tumor interior (inflammatory cells) (Figure 5). The initial study of the NPRC positive inflammatory cells inside the tumor showed co-localization with CD31 (Figure S5), confirming the presence of NPRC receptor during tumor angiogenesis and indicating its important role as diagnostic biomarker for tumorigenesis.[43,44]

CONCLUSION

Through controlled synthesis and assembly, a CANF peptide conjugated polymeric nanoparticle was prepared with tuned physicochemical and biological properties for PCa PET imaging. Immunohistochemistry confirmed the up-regulation of NPRC receptor in this

CWR22 tumor model. Initial *in vivo* evaluation demonstrated the superiority of targeted imaging over passive EPR effect in oncological diagnosis. The optimized *in vivo* pharmacokinetics, high sensitivity and specificity make ^{64}Cu-CANF-Comb candidate for PCa PET imaging.

Supplementary Material

Refer to Web version on PubMed Central for supplementary material.

Acknowledgments

We thank Terry Sharp, Nicole Fettig, Margaret Morris, Amanda Roth, Lori Strong, and Ann Stroncek for their assistance with animal imaging studies; and Tom Voller, Paul Eisenbies, and Evelyn Madrid for ^{64}Cu production. This work was supported by the National Institutes of Health as a Program of Excellence in Nanotechnology (HHSN268201000046C) (EP, RP, LAC, CJH and YL) and the National Science Foundation through the MRSEC program (DMR-1121053 – EP, LAC and CJH). We are grateful for funding support from Mallinckrodt Institute of Radiology, Washington University School of Medicine. The production of ^{64}Cu is supported by the National Cancer Institute (CA86307) with morphological studies and immunohistochemistry being supported by NIH/NHLBI PO1 HL29594.

LIST OF ABBREVIATION

ANP	atrial natriuretic peptide
CANF	C-atrial natriuretic factor
CT	computed tomography
DOTA	1,4,7,10-tetraazacyclododecane-1,4,7,10-tetraacetic acid
DO3A	1,4,7,10-tetraazacyclododecane-1,4,7-tris(*t*-butyl acetate)
EDTA	ethylene diamine tetraacetic acid
EPR	enhanced permeation and retention
FDG	fluoro-2-deoxy-2-D-glucose
FPLC	fast protein liquid chromatography
GPC	gel permeation chromatography
IHC	immunohistochemistry
ITLC	instant thin layer chromatography
MRI	magnetic resonance imaging
NMR	nuclear magnetic resonance
NPRA	natriuretic peptide receptor A
NPRC	natriuretic peptide clearance receptor
PCa	prostate cancer
PEG	poly ethylene glycol
PEGMA	poly(ethylene glycol) methyl ether mathacrylate
PET	positron emission tomography
RAFT	radical addition fragmentation transfer
ROI	region of interest

SPECT	single photon emission computed tomography
SUV	standardized uptake value
T/B	tumor-to-blood
T/K	tumor-to-kidney
T/M	tumor-to-muscle

REFERENCES

1. Siegel R, Naishadham D, Jemal A. Cancer statistics, 2012. CA Cancer J. Clin. 2012; 62:10–29. [PubMed: 22237781]
2. Turkbey B, Pinto PA, Choyke PL. Imaging techniques for prostate cancer: implications for focal therapy. Nat. Rev. Urol. 2009; 6:191–203. [PubMed: 19352394]
3. Pinto F, Totaro A, Palermo G, Calarco A, Sacco E, D'Addessi A, Racioppi M, Valentini A, Gui B, Bassi P. Imaging in prostate cancer staging: present role and future perspectives. Urol. Int. 2012; 88:125–136. [PubMed: 22286304]
4. Ravizzini G, Turkbey B, Kurdziel K, Choyke PL. New horizons in prostate cancer imaging. Eur. J. Radiol. 2009; 70:212–226. [PubMed: 18993004]
5. Lawrence EM, Gnanapragasam VJ, Priest AN, Sala E. The emerging role of diffusion-weighted MRI in prostate cancer management. Nat. Rev. Urol. 2012; 9:94–101. [PubMed: 22249194]
6. Bouchelouche K, Turkbey B, Choyke P, Capala J. Imaging prostate cancer: an update on positron emission tomography and magnetic resonance imaging. Curr. Urol. Rep. 2010; 11:180–190. [PubMed: 20425625]
7. Lears KA, Ferdani R, Liang K, Zheleznyak A, Andrews R, Sherman CD, Achilefu S, Anderson CJ, Rogers BE. In vitro and in vivo evaluation of 64Cu-labeled SarArbombesin analogs in gastrin-releasing peptide receptor-expressing prostate cancer. J. Nucl. Med. 2011; 52:470–477. [PubMed: 21321264]
8. Jackson AB, Nanda PK, Rold TL, Sieckman GL, Szczodroski AF, Hoffman TJ, Chen X, Smith CJ. 64Cu-NO2A-RGD-Glu-6-Ahx-BBN(7-14)NH2: a heterodimeric targeting vector for positron emission tomography imaging of prostate cancer. Nucl. Med. Biol. 2012; 39:377–387. [PubMed: 22226021]
9. Graham MM, Menda Y. Radiopeptide imaging and therapy in the United States. J. Nucl. Med. 2011; 52(Suppl 2):56S–63S. [PubMed: 22144556]
10. Nanda PK, Pandey U, Bottenus BN, Rold TL, Sieckman GL, Szczodroski AF, Hoffman TJ, Smith CJ. Bombesin analogues for gastrin-releasing peptide receptor imaging. Nucl. Med. Biol. 2012; 39:461–471. [PubMed: 22261143]
11. Chen Y, Pullambhatla M, Foss CA, Byun Y, Nimmagadda S, Senthamizhchelvan S, Sgouros G, Mease RC, Pomper MG. 2-(3-{1-Carboxy-5-[(6-[18F]fluoro-pyridine-3- carbonyl)-amino]-pentyl}-ureido)-pen tanedioic acid, [18F]DCFPyL, a PSMA-based PET imaging agent for prostate cancer. Clin. Cancer Res. 2011; 17:7645–7653. [PubMed: 22042970]
12. Lutje S, Boerman OC, van Rij CM, Sedelaar M, Helfrich W, Oyen WJ, Mulders PF. Prospects in radionuclide imaging of prostate cancer. Prostate. 2012; 72:1262–1272. [PubMed: 22127918]
13. Craft JM, De Silva RA, Lears KA, Andrews R, Liang K, Achilefu S, Rogers BE. In vitro and in vivo evaluation of a 64Cu-labeled NOTA-Bn-SCN-Aoc-bombesin analogue in gastrin-releasing peptide receptor expressing prostate cancer. Nucl. Med. Biol. 2012; 39:609–616. [PubMed: 22261146]
14. Liu Y, Welch MJ. Nanoparticles labeled with positron emitting nuclides: advantages, methods, and applications. Bioconjug. Chem. 2012; 23:671–682. [PubMed: 22242601]
15. Talekar M, Kendall J, Denny W, Garg S. Targeting of nanoparticles in cancer: drug delivery and diagnostics. Anticancer Drugs. 2011; 22:949–962. [PubMed: 21970851]
16. Kievit FM, Zhang M. Cancer nanotheranostics: improving imaging and therapy by targeted delivery across biological barriers. Adv. Mater. 2011; 23:H217–H247. [PubMed: 21842473]

17. Steinmetz NF, Ablack AL, Hickey JL, Ablack J, Manocha B, Mymryk JS, Luyt LG, Lewis JD. Intravital imaging of human prostate cancer using viral nanoparticles targeted to gastrin-releasing Peptide receptors. Small. 2011; 7:1664–1672. [PubMed: 21520408]

18. Chanda N, Kattumuri V, Shukla R, Zambre A, Katti K, Upendran A, Kulkarni RR, Kan P, Fent GM, Casteel SW, Smith CJ, Boote E, Robertson JD, Cutler C, Lever JR, Katti KV, Kannan R. Bombesin functionalized gold nanoparticles show in vitro and in vivo cancer receptor specificity. Proc. Natl. Acad. Sci. U. S. A. 2010; 107:8760–8765. [PubMed: 20410458]

19. Mendoza-Sanchez AN, Ferro-Flores G, Ocampo-Garcia BE, Morales-Avila E, de MRF, De Leon-Rodriguez LM, Santos-Cuevas CL, Medina LA, Rojas-Calderon EL, Camacho- Lopez MA. Lys3-bombesin conjugated to 99mTc-labelled gold nanoparticles for in vivo gastrin releasing peptide-receptor imaging. J Biomed. Nanotechnol. 2010; 6:375–384. [PubMed: 21323111]

20. Becker AL, Orlotti NI, Folini M, Cavalieri F, Zelikin AN, Johnston AP, Zaffaroni N, Caruso F. Redox-active polymer microcapsules for the delivery of a survivin-specific siRNA in prostate cancer cells. ACS Nano. 2011; 5:1335–1344. [PubMed: 21226510]

21. Maack T. The broad homeostatic role of natriuretic peptides. Arq Bras Endocrinol Metabol. 2006; 50:198–207. [PubMed: 16767286]

22. Wang X, Raulji P, Mohapatra SS, Patel R, Hellermann G, Kong X, Vera PL, Meyer- Siegler KL, Coppola D, Mohapatra S. Natriuretic peptide receptor a as a novel target for prostate cancer. Mol. Cancer. 2011; 10:56–67. [PubMed: 21586128]

23. Sun Y, Eichelbaum EJ, Wang H, Vesely DL. Atrial natriuretic peptide and long acting natriuretic peptide inhibit MEK 1/2 activation in human prostate cancer cells. Anticancer Res. 2007; 27:3813–3818. [PubMed: 18225537]

24. Sun Y, Eichelbaum EJ, Lenz A, Skelton WPt, Wang H, Vesely DL. Atrial natriuretic peptide and long-acting natriuretic peptide inhibit ras in human prostate cancer cells. Anticancer Res. 2009; 29:1889–1893. [PubMed: 19528444]

25. Kong X, Wang X, Xu W, Behera S, Hellermann G, Kumar A, Lockey RF, Mohapatra S, Mohapatra SS. Natriuretic peptide receptor a as a novel anticancer target. Cancer Res. 2008; 68:249–256. [PubMed: 18172317]

26. Terada N, Shimizu Y, Kamba T, Inoue T, Maeno A, Kobayashi T, Nakamura E, Kamoto T, Kanaji T, Maruyama T, Mikami Y, Toda Y, Matsuoka T, Okuno Y, Tsujimoto G, Narumiya S, Ogawa O. Identification of EP4 as a potential target for the treatment of castrationresistant prostate cancer using a novel xenograft model. Cancer Res. 2010; 70:1606–1615. [PubMed: 20145136]

27. Vesely BA, Alli AA, Song SJ, Gower WR Jr, Sanchez-Ramos J, Vesely DL. Four peptide hormones' specific decrease (up to 97%) of human prostate carcinoma cells. Eur. J. Clin. Invest. 2005; 35:700–710. [PubMed: 16269020]

28. Shokeen M, Pressly ED, Hagooly A, Zheleznyak A, Ramos N, Fiamengo AL, Welch MJ, Hawker CJ, Anderson CJ. Evaluation of multivalent, functional polymeric nanoparticles for imaging applications. ACS Nano. 2011; 5:738–747. [PubMed: 21275414]

29. Pressly ED, Rossin R, Hagooly A, Fukukawa K, Messmore BW, Welch MJ, Wooley KL, Lamm MS, Hule RA, Pochan DJ, Hawker CJ. Structural effects on the biodistribution and positron emission tomography (PET) imaging of well-defined (64)Cu-labeled nanoparticles comprised of amphiphilic block graft copolymers. Biomacromolecules. 2007; 8:3126–3134. [PubMed: 17880180]

30. Nagabhushan M, Miller CM, Pretlow TP, Giaconia JM, Edgehouse NL, Schwartz S, Kung HJ, de Vere White RW, Gumerlock PH, Resnick MI, Amini SB, Pretlow TG. CWR22: the first human prostate cancer xenograft with strongly androgen-dependent and relapsed strains both in vivo and in soft agar. Cancer Res. 1996; 56:3042–3046. [PubMed: 8674060]

31. Dyke JP, Zakian KL, Spees WM, Matei C, Chen Y, Mao X, Shungu DC, Koutcher JA. Metabolic response of the CWR22 prostate tumor xenograft after 20 Gy of radiation studied by 1H spectroscopic imaging. Clin. Cancer Res. 2003; 9:4529–4536. [PubMed: 14555527]

32. Roe K, Mikalsen LT, van der Kogel AJ, Bussink J, Lyng H, Ree AH, Marignol L, Olsen DR. Vascular responses to radiotherapy and androgendeprivation therapy in experimental prostate cancer. Radiat. Oncol. 2012; 7:75. [PubMed: 22621752]

33. Ponde DE, Dence CS, Oyama N, Kim J, Tai YC, Laforest R, Siegel BA, Welch MJ. 18F-fluoroacetate: a potential acetate analog for prostate tumor imaging--in vivo evaluation of 18F-fluoroacetate versus 11C-acetate. J. Nucl. Med. 2007; 48:420–428. [PubMed: 17332620]
34. McCarthy DW, Shefer RE, Klinkowstein RE, Bass LA, Margeneau WH, Cutler CS, Anderson CJ, Welch MJ. Efficient production of high specific activity 64Cu using a biomedical cyclotron. Nucl. Med. Biol. 1997; 24:35–43. [PubMed: 9080473]
35. Herrero P, Kim J, Sharp TL, Engelbach JA, Lewis JS, Gropler RJ, Welch MJ. Assessment of myocardial blood flow using 15O-water and 1-11C-acetate in rats with smallanimal PET. J. Nucl. Med. 2006; 47:477–485. [PubMed: 16513617]
36. Liu Y, Ibricevic A, Cohen JA, Cohen JL, Gunsten SP, Frechet JM, Walter MJ, Welch MJ, Brody SL. Impact of hydrogel nanoparticle size and functionalization on in vivo behavior for lung imaging and therapeutics. Mol. Pharm. 2009; 6:1891–1902. [PubMed: 19852512]
37. Almutairi A, Rossin R, Shokeen M, Hagooly A, Ananth A, Capoccia B, Guillaudeu S, Abendschein D, Anderson CJ, Welch MJ, Frechet JM. Biodegradable dendritic positron-emitting nanoprobes for the noninvasive imaging of angiogenesis. Proc. Natl. Acad. SciUSA. 2009; 106:685–690.
38. Liu Y, Abendschein D, Woodard GE, Rossin R, McCommis K, Zheng J, Welch MJ, Woodard PK. Molecular imaging of atherosclerotic plaque with (64)Cu-labeled natriuretic peptide and PET. J. Nucl. Med. 2010; 51:85–91. [PubMed: 20008978]
39. Liu Y, Pressly ED, Abendschein DR, Hawker CJ, Woodard GE, Woodard PK, Welch MJ. Targeting angiogenesis using a C-type atrial natriuretic factor-conjugated nanoprobe and PET. J. Nucl. Med. 2011; 52:1956–1963. [PubMed: 22049461]
40. Rogers BE, Bigott HM, McCarthy DW, Della Manna D, Kim J, Sharp TL, Welch MJ. MicroPET imaging of a gastrin-releasing peptide receptor-positive tumor in a mouse model of human prostate cancer using a 64Cu-labeled bombesin analogue. Bioconjug. Chem. 2003; 14:756–763. [PubMed: 12862428]
41. Ting G, Chang CH, Wang HE. Cancer nanotargeted radiopharmaceuticals for tumor imaging and therapy. Anticancer Res. 2009; 29:4107–4118. [PubMed: 19846958]
42. Rubattu S, Sciarretta S, Morriello A, Calvieri C, Battistoni A, Volpe M. NPR-C: a component of the natriuretic peptide family with implications in human diseases. J. Mol. Med. (Berl). 2010; 88:889–897. [PubMed: 20563546]
43. Bergers G, Benjamin LE. Tumorigenesis and the angiogenic switch. Nat. Rev. Cancer. 2003; 3:401–410. [PubMed: 12778130]
44. Dudley AC. Tumor endothelial cells. Cold Spring Harb Perspect Med. 2012; 2:a006536. [PubMed: 22393533]

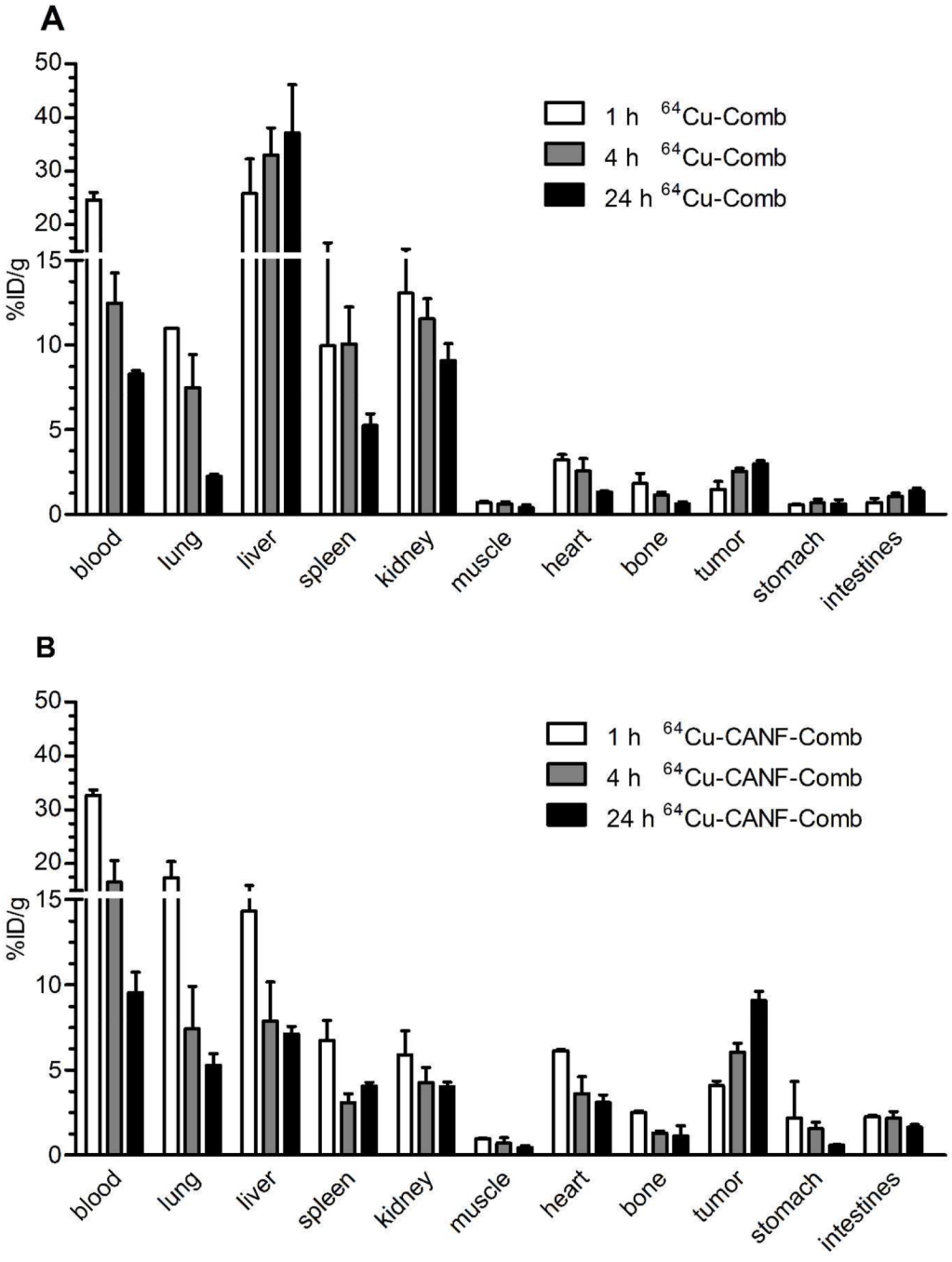

Figure 1.

Biodistribution of ^{64}Cu-Comb and ^{64}Cu-CANF-Comb in CWR22 tumor model following intravenous injection (n=4/group). (A) ^{64}Cu-Comb showing low tumor accumulation but high liver uptake. (B) ^{64}Cu-CANF-Comb showing high tumor localization and superior pharmacokinetics relative to ^{64}Cu-Comb with high blood retention and low hepatic burden.

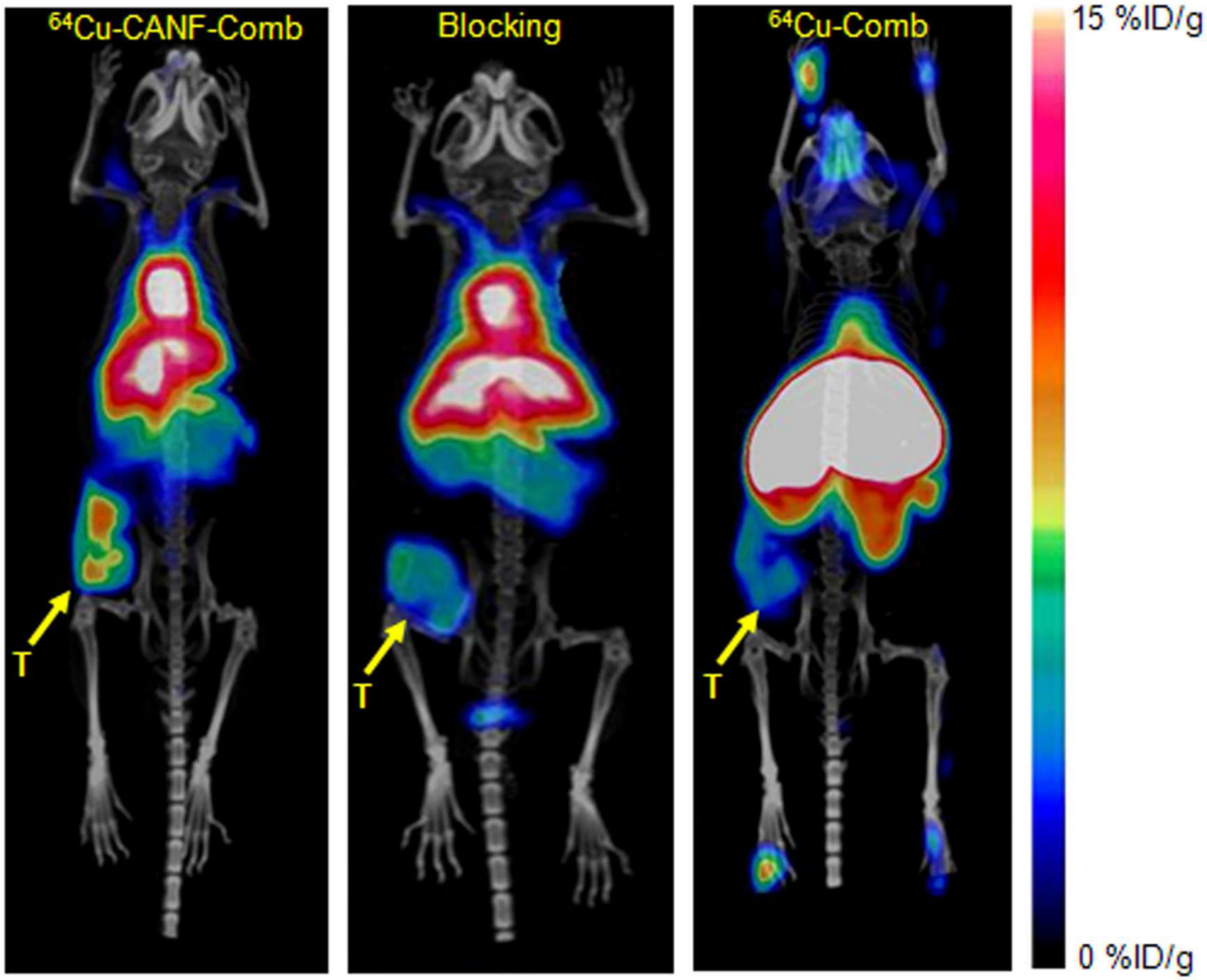

Figure 2.
PET/CT images of ^{64}Cu-CANF-Comb, ^{64}Cu-CANF-Comb blocking and ^{64}Cu-Comb in CWR 22 tumor at 24 h post injection. T: tumor

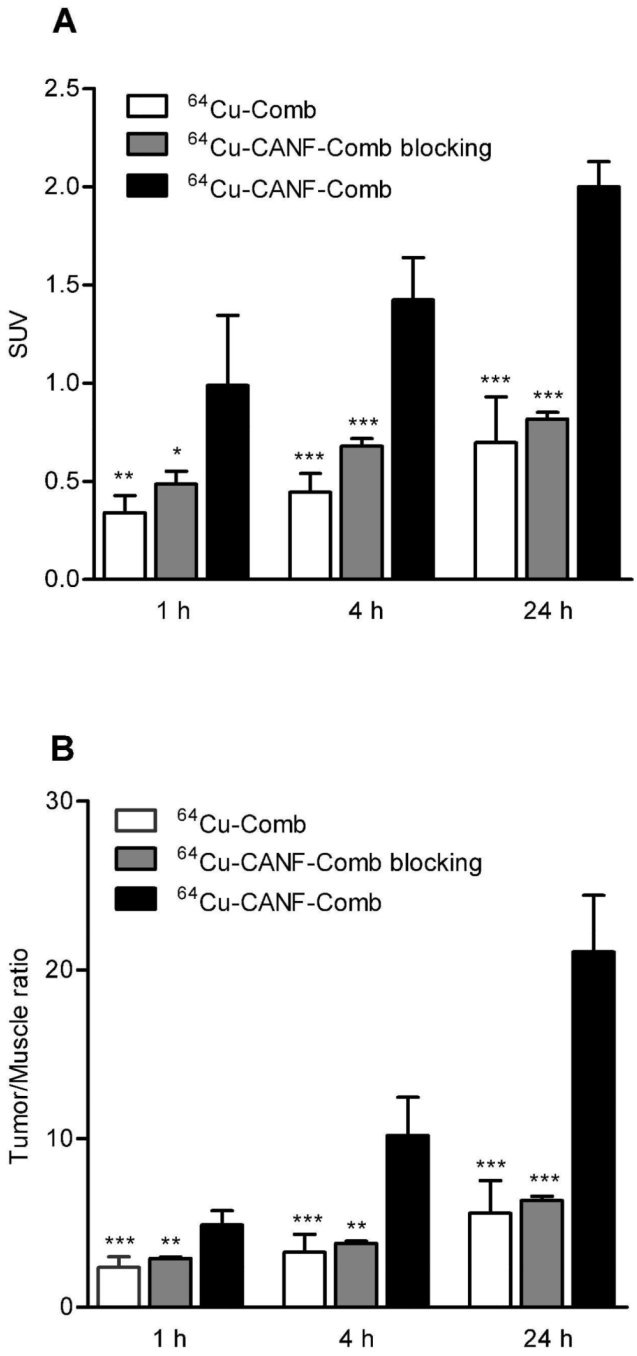

Figure 3.

(A) Quantitative tumor uptake SUVs and tumor/muscle uptake ratios of ^{64}Cu-Comb, ^{64}Cu-CANF-Comb and ^{64}Cu-CANF-Comb blocking in CWR 22 tumor at three different time points (n=6–8/group) (statistical analysis of ^{64}Cu-Comb and ^{64}Cu-CANF-Comb blocking compared to ^{64}Cu-CANF-Comb; *: $p<0.05$; **: $p<0.001$; ***: $p<0.0001$).

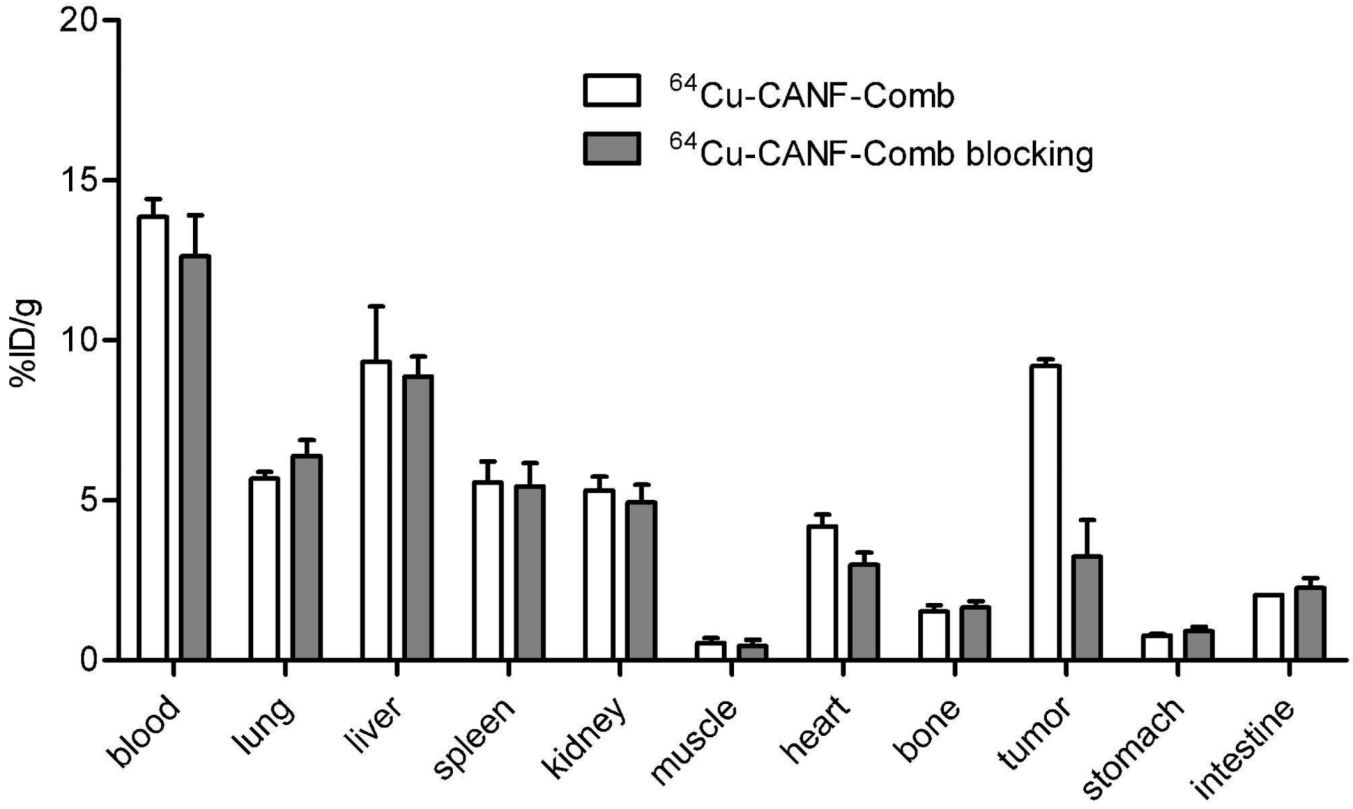

Figure 4.
Biodistribution of ^{64}Cu-CANF-Comb and ^{64}Cu-CANF-Comb blocking in CWR 22 tumor model at 24 h post injection (n=4/group, blockade : ^{64}Cu-CANF-Comb = 100:1).

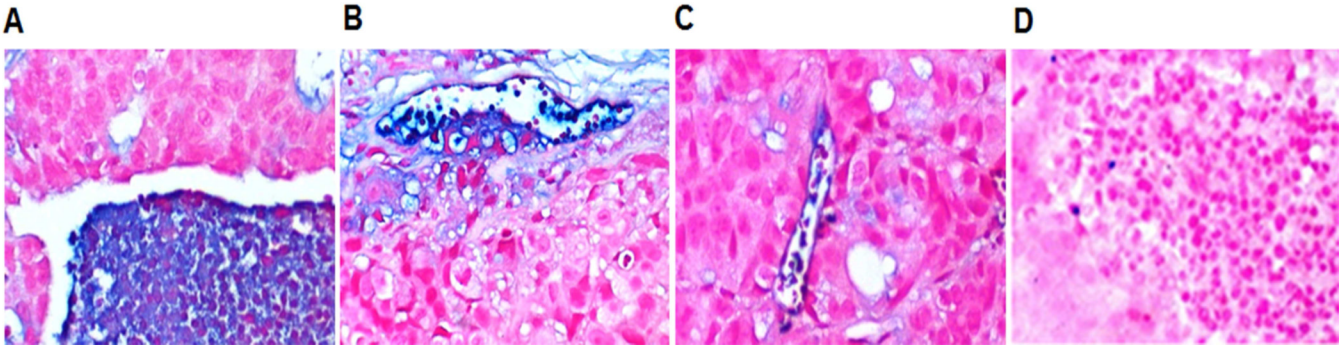

Figure 5.
Immunohistochemical staining of NPRC receptor (blue) in tumor tissue (counterstained with nuclear fast red). (A) High expression of NPRC in pools of inflammatory cells within the tumor. (B) NPRC found in inflammatory cells and in the endothelial lining of small vessels in the tumor periphery. (C) NPRC staining of the endothelial wall and some inflammatory cells in a peripheral vessel within the tumor. (D) Section incubated with pre-immune serum instead of primary antibody. All panels are at 200×.

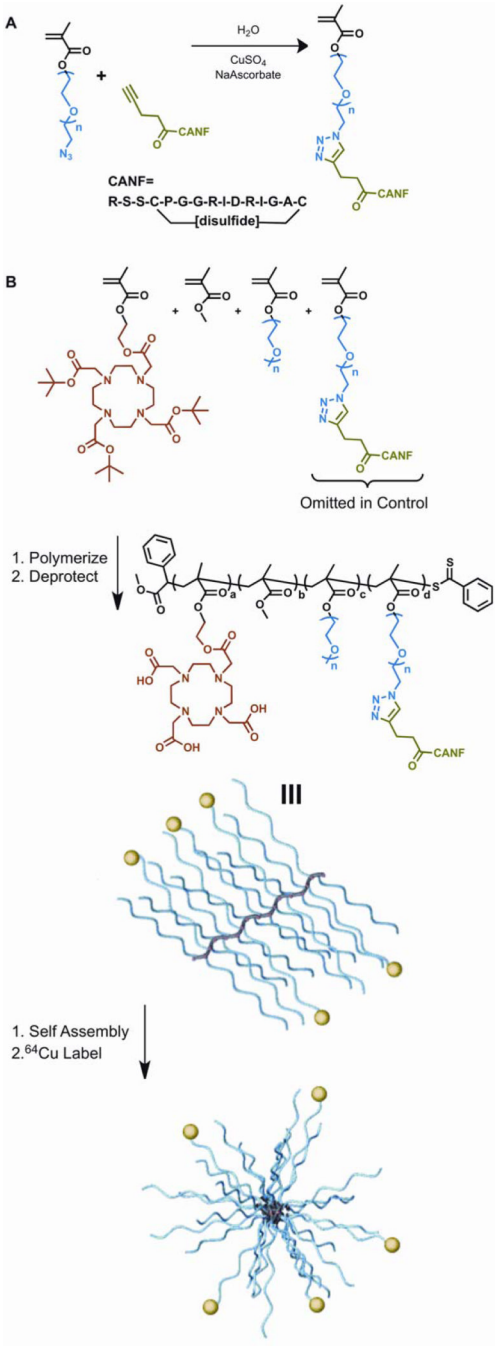

Scheme 1.
(A) Synthesis of CANF-PEG-methacrylate monomer via “Click” chemistry. (B) Synthesis of CANF-Comb, deprotection and subsequent assembly into nanoparticles.